doi:10.1093/jmcb/mjab036
Published online June 18, 2021

Article

The septin complex links the catenin complex to the actin cytoskeleton for establishing epithelial cell polarity

Xueying Wang[1,2], Wenwen Wang [1,2,3], Xiwei Wang[1,2], Ming Wang[1], Lijuan Zhu[1,3], Fatima Garba[2], Chuanhai Fu[1,3], Barbara Zieger[4,*], Xu Liu[1,2,*], Xing Liu [1,3,*], and Xuebiao Yao[1,3]

[1] MOE Key Laboratory for Membraneless Organelles & Cellular Dynamics and Hefei National Laboratory for Physical Sciences at the Microscale, University of Science and Technology of China, Hefei 230027, China
[2] Keck Center for Organoids Plasticity Control, Atlanta, GA 30310, USA
[3] Anhui Key Laboratory for Cellular Dynamics & Chemical Biology and CAS Center for Excellence in Molecular Cell Science, Hefei 230027, China
[4] Department of Pediatrics and Adolescent Medicine, Division of Pediatric Hematology and Oncology, Medical Center, Faculty of Medicine, University of Freiburg, 79106 Freiburg, Germany
* Correspondence to: Barbara Zieger, E-mail: barbara.zieger@uniklinik-freiburg.de; Xu Liu, E-mail: lxu1016@ustc.edu.cn; Xing Liu, E-mail: xing1017@ustc.edu.cn

Edited by Haian Fu

Cell polarity is essential for spatially regulating of physiological processes in metazoans by which hormonal stimulation–secretion coupling is precisely coupled for tissue homeostasis and organ communications. However, the molecular mechanisms underlying epithelial cell polarity establishment remain elusive. Here, we show that septin cytoskeleton interacts with catenin complex to organize a functional domain to separate apical from basal membranes in polarized epithelial cells. Using polarized epithelial cell monolayer as a model system with transepithelial electrical resistance as functional readout, our studies show that septins are essential for epithelial cell polarization. Our proteomic analyses discovered a novel septin–catenin complex during epithelial cell polarization. The functional relevance of septin–catenin complex was then examined in three-dimensional (3D) culture in which suppression of septins resulted in deformation of apical lumen in cysts, a hallmark seen in polarity-deficient 3D cultures and animals. Mechanistically, septin cytoskeleton stabilizes the association of adherens catenin complex with actin cytoskeleton, and depletion or disruption of septin cytoskeleton liberates adherens junction and polarity complexes into the cytoplasm. Together, these findings reveal a previously unrecognized role for septin cytoskeleton in the polarization of the apical–basal axis and lumen formation in polarized epithelial cells.

Keywords: septin, cytoskeleton, cell polarity, adherens junction, epithelial cells

Introduction

Epithelia are the most archetypal polarized tissues in metazoans during phylogenesis, which comprise the foundation for the majority of secretory organs in the mammalian body (Rodriguez-Boulan and Macara, 2014). Many epithelial organs consist of tubes of epithelial cells enclosing a central lumen, such as gastrointestinal and renal tissues (Bryant and Mostov, 2008; Odenwald et al., 2017), whose organization mostly depends on apical–basal polarity to distinguish the outside surface from the inside surface of the sheet (O'Brien et al., 2002; Bryant and Mostov, 2008; Odenwald et al., 2017). Conversely, the disruption of polarity in epithelial cells often compromised the defense system against pathogen invasion, such as *Helicobacter pylori* and SARS-CoV-2 infection (McCaffrey and Macara, 2011; Sousa et al., 2019). During epithelial polarity establishment, cell–cell junctions are organized by adhesion proteins and the underlying actin cytoskeleton (Li and Gundersen, 2008; Campos et al., 2016; Dogterom and Koenderink, 2019). However, how the cytoskeleton orchestrates apical–basal polarity establishment is a key question in morphogenesis.

Septins are guanosine-5′-triphosphate (GTP)-binding proteins belonging to a family of proteins that are highly

Received November 25, 2020. Revised March 16, 2021. Accepted March 23, 2021.
© The Author(s) (2021). Published by Oxford University Press on behalf of *Journal of Molecular Cell Biology*, CEMCS, CAS.
This is an Open Access article distributed under the terms of the Creative Commons Attribution Non-Commercial License (http://creativecommons.org/licenses/by-nc/4.0/), which permits non-commercial re-use, distribution, and reproduction in any medium, provided the original work is properly cited. For commercial re-use, please contact journals.permissions@oup.com

conserved in eukaryotes. There are 13 encoded septins in humans (SEPT1–SEPT12 and SEPT14). Based on homology of sequence and protein domains, septins can be classified into four subgroups, namely the SEPT2, SEPT3, SEPT6, and SEPT7 subgroups (Kinoshita, 2003; Mostowy and Cossart, 2012; Neubauer and Zieger, 2017). SEPT7 is thought to be a unique and perhaps irreplaceable subunit that binds to SEPT2 and SEPT6 subfamily members, which can assemble into hetero-oligomeric complexes and higher-order structures, including filaments and rings (Mostowy and Cossart, 2012; Torraca and Mostowy, 2016). Our early studies show that septin network orchestrates accurate mitotic cell division from chromosome segregation to cytokinesis (Zhu et al., 2008; Zheng et al., 2018). Septins have been recognized as the fourth component of the cytoskeleton because of their filamentous appearance and their association with cellular membranes, actin filaments, and microtubules (Mostowy and Cossart, 2012; Pous et al., 2016), which play important roles in orchestrating cellular processes. Previously studies have shown that in budding yeast, septins recruit membrane proteins to cleavage furrow during asymmetric cell division to determine cell polarity (McMurray and Thorner, 2009) and also provide birthmark for neuron division (Boubakar et al., 2017). In the mammalian epithelial cells, SEPT2 spatially organizes the growth and apicobasal distribution of microtubule network (Bowen et al., 2011). In addition, SEPT2 antagonizes MAP4 from microtubules and associates with polyglutamylated tubulin cytoskeleton, therefore regulating the efficiency of post-Golgi vesicle transport and columnar-shaped polarized epithelia (Spiliotis et al., 2008). Recent work showed that in endothelial cells, SEPT2 associates with actin filaments and VE-cadherin to orchestrate the integrity of cell junction and barrier function (Sidhaye et al., 2011; Kim and Cooper, 2018). However, in contrast with actin and microtubules, relatively little is known about the role and mechanism of action underlying septin-mediated epithelial apical–basal polarity establishment.

Here, we show that human septin cytoskeleton is localized to the lateral membrane in polarized epithelial cells. Biochemically, septins interact with catenin complex and serve as a link between catenin complex and actin filaments. Importantly, septins are essential for accurate lumen formation during cyst maturation in three-dimensional (3D) culture. Thus, septin–catenin interaction provides a spatiotemporal link between epithelial apical–basal polarity establishment and glandular lumen formation.

Results

Septins are essential for epithelial polarity establishment

Our early studies show that SEPT7 forms a link between kinetochore distribution of CENP-E and the mitotic spindle checkpoint (Zhu et al., 2008). Given the polarity establishment after mitotic exit, we sought to examine the precise function of SEPT7 in cell polarity establishment. To this end, 3D culture system of Caco-2 cell cysts was established and infected with lentiviral-based shRNA to suppress various septin protein expressions. As shown in Supplementary Figure S1A, infection of shSEPT7 resulted in time-dependent suppression of septin protein levels with an optimal time at 72 h postinfection.

To examine whether all of septin members were required for cyst formation, we carried out immunofluorescence microscopic analysis of 3D cysts by examination of apical and lateral membrane markers. As shown in Figure 1A, Caco-2 cells embedded in Matrigel developed into well-organized cysts on Day 6, which was hallmarked by the apical localization of ezrin, an actin-based cytoskeletal linker essential for apical polarity establishment and dynamic membrane–cytoskeletal remodeling (Yao et al., 1996; Bisaria et al., 2020). Almost all cysts in the control group exhibit characteristic open lumen, the hallmark of polarized 3D cell culture, by which ezrin distribution exhibits ring-like structure marking the interconnected apical membrane of Caco-2 cells. As shown in Figure 1A (top panel), the adherens junction maker β-catenin is distributed mainly at the lateral membrane of polarized Caco-2 cells, which is readily apparent in magnified image (Figure 1B). Higher magnification of the merged image revealed polarized distribution of ezrin and β-catenin, which is characteristic of mature cyst (Figure 1B).

We next examined the distribution pattern of ezrin relative to β-catenin in septin-suppressed cysts achieved by shRNA-mediated knockdown. Surprisingly, examination of shSEPT-treated crest in the same batch revealed that a typical phenotype of no-lumen given the collapse of hollow crests (Figure 1A, middle and lower panels). Careful examination of the merged image revealed that collapse of lumen exhibited disorganization of cellular polarity as ezrin and β-catenin became aggregated (Figure 1A, lower panels). Further examination of enlarged image of septin-suppressed cysts indicated that suppression of SEPT7 resulted in phenotypes including multilumen, no-lumen, and small cyst, which reflects the importance of SEPT7 in polarity establishment. Our statistical analyses show that suppression of SEPT2/6/7 perturbed lumen sealing, which is evident by no-lumen or multilumen cysts (Figure 1C).

To characterize whether the delocalization of β-catenin is a result of lost SEPT7 scaffold, we carried out western blotting analysis of β-catenin in shRNA-treated cysts. Our analyses show that the protein expression level of β-catenin and ezrin has no change, suggesting that the observed delocalization of β-catenin was not due to its protein degradation. To probe the interrelationship among three septin isoforms, we carried out western blotting analysis to examine whether suppression of one septin isoform affects the expression of the other two isoforms, as SEPT2/6/7 exists as a hetero-hexamer. As shown in Figure 1D, suppression of SEPT7 by shRNA resulted in a reduction of SEPT7 protein level in addition to destabilized SEPT2 and SEPT6 protein levels in Caco-2 cells. This line of observation is consistent with studies in HeLa cells and MDCK cells (Kremer et al., 2005, 2007; Sellin et al., 2011), in which SEPT7 functions as an integral filamentous complex (Sirajuddin et al., 2007). Thus, we conclude that perturbation of SEPT2/6/7 functional integrity by suppression of SEPT7

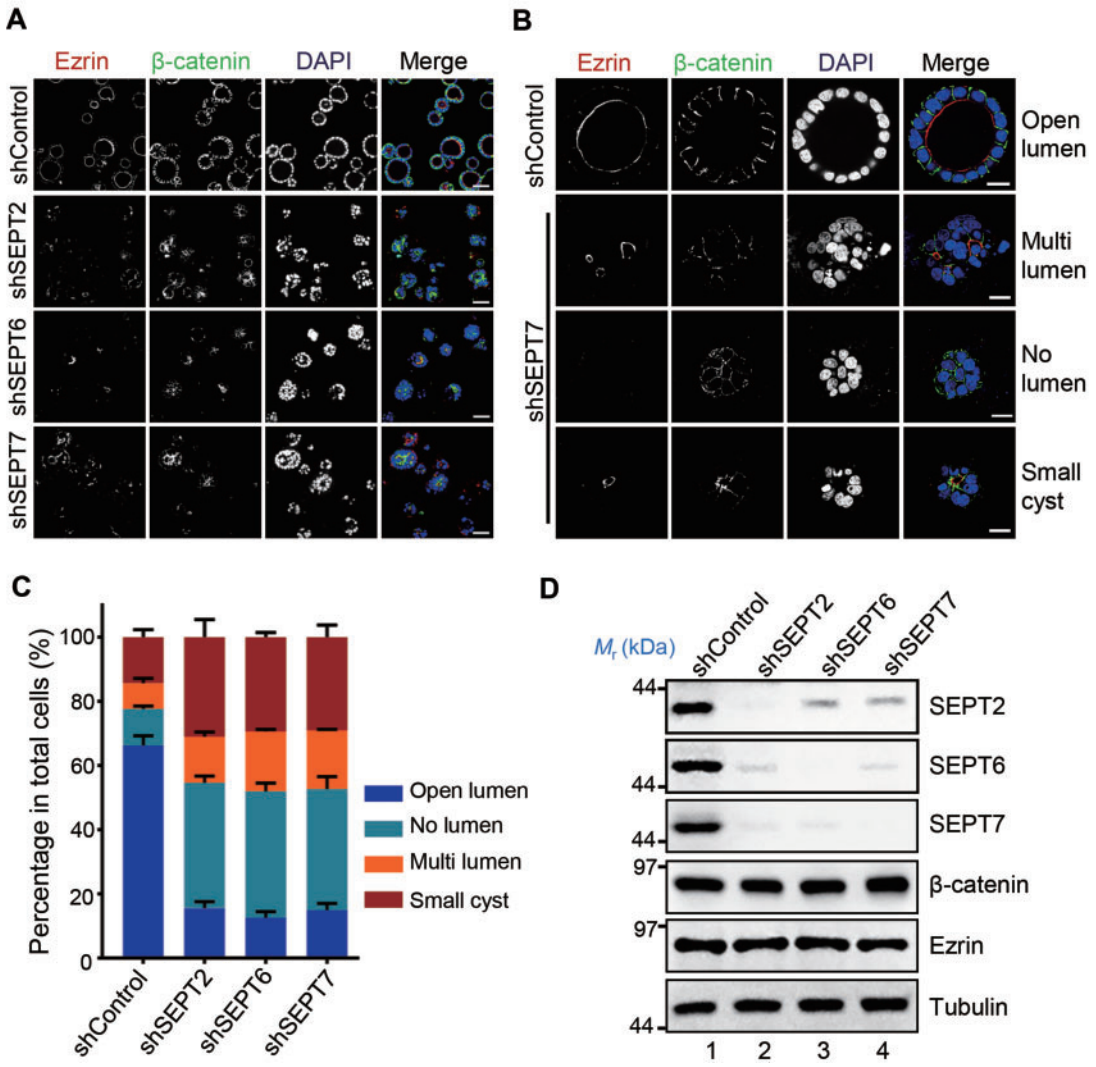

Figure 1 Septins regulate Caco-2 cyst morphogenesis. (**A**) Caco-2 cells were infected with control shRNA or shSEPT2, shSEPT6, and shSEPT7 lentiviruses, respectively, and then plated in Matrigel to allow cystogenesis. cysts were grown for 6 days and presented different phenotypes, which were identified by the apical membrane maker ezrin (red), the adherens junction maker β-catenin (green), and DAPI (blue). A confocal section through the middle region of the cyst using 20× objectives is shown. Scale bar, 20 μm. (**B**) Representative phenotypes in control and SEPT7-depleted cysts from **A** labelled for ezrin (red) and β-catenin (green) as indicated. Three representative phenotypes of luminal abnormalities were observed in shSEPT7 cysts (multilumen, no-lumen, and small cysts). A confocal section through the middle of the cyst using 63× objectives is shown. Scale bar, 20 μm. (**C**) Quantification of cyst phenotypes in **A**. Cysts organized by Caco-2 cells infected with control shRNA lentivirus ($n = 100$), shSEPT2 lentivirus ($n = 120$), shSEPT6 lentivirus ($n = 120$), and shSEPT7 lentivirus ($n = 120$), respectively. Data represent mean ± standard error of the mean (SEM) from three independent experiments. (**D**) Representative western blotting analysis of shSEPT2, shSEPT6, and shSEPT7 lentivirus-mediated knockdown efficiency for real-time imaging experiment shown in **A**.

protein level resulted in the perturbation of accurate lumen formation.

To validate the significance of septins in epithelial polarity establishment, we introduced a septin filament inhibitory compound forchlorfenuron (FCF) into 3D culture of Caco-2 cells. FCF is a membrane-permeable compound that disrupts the polymerization of SEPT2/6/7 *in vivo* (Hu et al., 2008). To assess whether septin cytoskeleton is critical for epithelial polarization, we introduced FCF into the culture media during the process of cyst formation. Similar to what was observed in septin-suppressed cysts, characteristic lumen structure was perturbed in the presence of FCF, while DMSO-treated cysts were morphologically matured, judged by immunofluorescence staining of actin and tubulin (Supplementary Figure S1B). We next assessed the effect of FCF on the maintenance of cell polarity by treating cysts with FCF after the cysts were fully formed. As shown in Supplementary Figure S1B, treatment of 6-day well-formed cysts with FCF for 24 h resulted in

the characteristic phenotype of no-lumen and multilumen cysts (Supplementary Figure S1C), indicating that septin function is essential for polarity maintenance. Thus, we conclude that SEPT7 complex is required for establishment and maintenance of epithelial apical–basal polarity during cyst morphogenesis.

Septin filaments localize at adherens junction in polarized epithelial cells

To delineate the mechanisms of action underlying septin cytoskeleton organization of epithelial polarity, we first examined the precise localization of septins using polarized Caco-2 monolayers (illustrated in Figure 2A and B). The two-dimensional

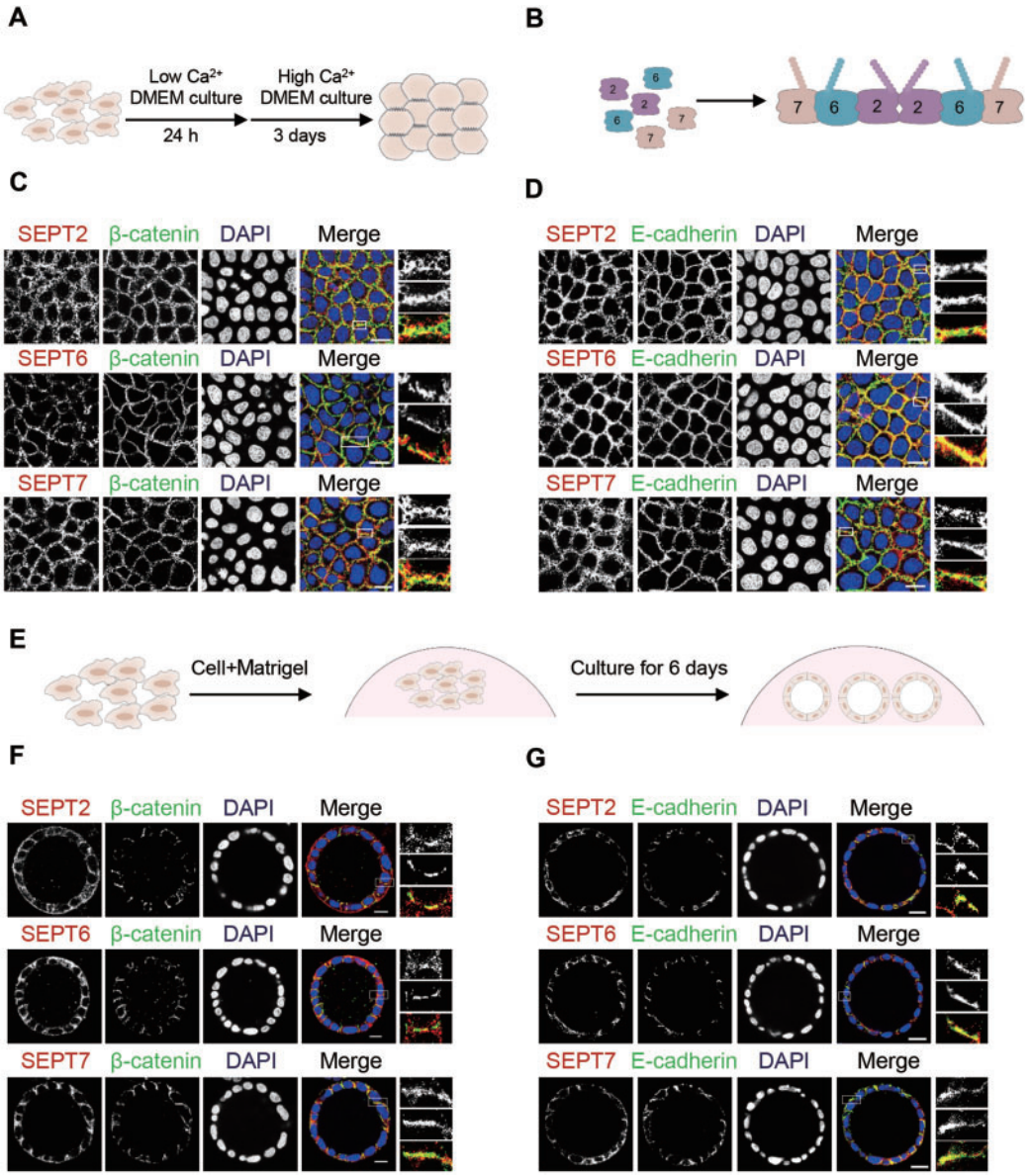

Figure 2 Septin filaments localize at adherens junction in polarized epithelial cells. (**A**) Schematic illustration of 2D cell culture. Caco-2 single cells were plated onto coverslip and grown for 3 days to form 100% confluent monolayers, which have distinct cell junction. (**B**) Schematic presentation of the organization of SEPT2/6/7 hetero-hexamer. (**C** and **D**) Representative immunofluorescence images of Caco-2 monolayers. Cells were fixed, permeabilized, and stained with anti-SEPT2/6/7 (red) and anti-β-catenin or anti-E-cadherin (green), respectively. Note that SEPT2/6/7 and adherens junction markers colocalize at cell junction. A single section through the middle of monolayers is shown. Scale bar, 20 μm. (**E**) Schematic presentation of 3D cell culture. Caco-2 single cells were seeded in Matrigel and grown for 6 days to allow cyst formation with an open lumen. (**F** and **G**) Representative immunofluorescence images of Caco-2 3D cysts. Cysts were fixed and stained with anti-SEPT2/6/7 (red) and anti-β-catenin or anti-E-cadherin (green). Note that SEPT2/6/7 and adherens junction markers colocalize at lateral membrane in 3D cyst model. A single confocal section through the middle of cysts was projected. Scale bar, 20 μm.

(2D) Caco-2 monolayers exhibit characteristic columnar shape showing distinct apical and basolateral membranes. We carried out confocal laser scanning of polarized cells from apical to basolateral membranes of cells labelled with SEPT2/6/7 and the adherens junction makers β-catenin/E-cadherin, respectively. As shown in Figure 2C and D, β-catenin and E-cadherin exhibited characteristic lateral labelling at cell–cell junction of polarized Caco-2 cells. Careful examination revealed a similar lateral labelling of SEPT2/6/7 which is superimposed onto that of β-catenin and E-cadherin. However, the localization of SEPT2/6/7 appeared less focused to the junctional complex compared to that of β-catenin and E-cadherin.

To further examine the precise localization of SEPT2/6/7 relative to that of the adherens junction makers β-catenin/E-cadherin in 3D cysts (illustrated in Figure 2E), we carried out confocal microscopic analysis of immunofluorescence-labelled Caco-2 cysts. As shown in Figure 2F, Caco-2 cells formed matured cyst in which lumen structure is fully developed and β-catenin exhibits characteristic lateral membrane distribution. Examination of SEPT2/6/7 staining in the β-catenin-marked cysts revealed superimposition of SEPT2/6/7 labelling onto that of β-catenin labelling. In addition, SEPT2/6/7 also distribute to basal membrane (Figure 2F). We next examined the distribution pattern of SEPT2/6/7 relative to that of E-cadherin. Consistent with what was seen in the β-catenin-marked cysts (Figure 2G), SEPT2/6/7 distribution is superimposed onto that of E-cadherin labelling at the lateral membrane. Thus, we conclude that majority of septin cytoskeleton is located at cell–cell junction of polarized 2D monolayers where E-cadherin and β-catenin are localized.

Septins are required for adherens junction integrity but not tight junction integrity

We next asked whether septins are required for the stability of cell–cell junction complex. To this end, we knocked down endogenous SEPT7 and examined the distribution of adherens junction proteins and tight junction proteins. Caco-2 cells were infected with shControl or shSEPT7 lentiviruses for 12 h followed by 2D polarization. Western blotting analyses showed that suppression of SEPT7 by shRNA resulted in a reduction of 92% ± 3% of SEPT7 protein (Figure 1D). The polarized cells were then fixed and stained for SEPT7 and E-cadherin followed by laser-scanning confocal microscopic analysis. As shown in Figure 3A, SEPT7 colocalizes with E-cadherin in control shRNA-treated cells. However, suppression of SEPT7 resulted in dramatic reduction of basolaterally distributed E-cadherin. We further examined the impact of SEPT7 suppression on the distribution of α/β-catenin and occludin, respectively. Consistent with the importance of SEPT7 in localizing α/β-catenin to the junctional complex, suppression of SEPT7 dramatically suppresses the lateral localization of α/β-catenin (Figure 3B and C). However, the localization of occludin to the lateral membrane is independent of SEPT7 (Figure 3D). As shown in Supplementary Figure S2, suppression of SEPT2 or SEPT6 also resulted in significant reduction of α/β-catenin and E-cadherin signal intensities, further confirming that SEPT2/6/7 form a functional complex to maintain adherens junction integrity.

To validate the impact of SEPT7 deficiency on E-cadherin and other junctional complex components, we carried out microscopic analysis of the Z sections according to our previous studies (Liu et al., 2007). Although SEPT7 and E-cadherin were detected predominantly in the lateral region in Caco-2 cells, as seen in the confocal apical X–Y section of the cell monolayer (Figure 3A), their colocalization to the lateral membrane was readily apparent when the Z sections were projected (Figure 3E). In addition, SEPT7 distribution to apical membrane was also observed when a minor fraction of SEPT7 was detected on the basal membrane of the cells as the Z sections were projected (Figure 3E). However, E-cadherin was no longer observed on the lateral membrane in shSEPT7-treated cells, suggesting that lateral localization of E-cadherin is a function of SEPT7.

We then scored the localization of α/β-catenin to the lateral membrane in shSEPT7-treated cells. As shown in Figure 3F and G, α/β-catenin localization to the lateral membrane was dramatically reduced. However, the localization of occludin to the lateral membrane was not altered by the suppression of SEPT7 (Figure 3H). Thus, septin cytoskeleton is essential for adherens junction establishment and stability, while the stability of tight junction was barely affected by the suppression of SEPT7. To validate that suppression of septins did not affect the stability of α/β-catenin and E-cadherin proteins, we carried out western blotting analysis on these cells. As shown in Figure 3I, the stability of α/β-catenin and E-cadherin proteins was not altered by the suppression of SEPT7. Thus, we propose that SEPT2/6/7 are necessary for adherens junction stability but not tight junction stability.

Junctional localization of septins depends on E-cadherin

E-cadherin-dependent adherens junction is a quaternary complex composing of the transmembrane protein E-cadherin, as well as the cytoplasmic proteins β-catenin and α-catenin. We next asked whether lateral distribution of septin filaments is regulated by adherens junction complex. To this end, we treated Caco-2 cells with shRNA followed by monolayer formation. As shown in Figure 4A, E-cadherin colocalizes with SEPT7 to the lateral membrane in polarized Caco-2 cells. Suppression of E-cadherin (E-cad) eliminated lateral localization of SEPT7, suggesting an interdependent relationship between SEPT7 and E-cadherin. However, suppression of β-catenin and α-catenin did not alter lateral localization of SEPT7, but the localization appeared less focused to the cell junction compared to control group (Figure 4B and C). We carried out confocal microscopic analysis of the Z sections as described above. As shown in Figure 4D, suppression of E-cadherin resulted in no lateral localization of SEPT7, which confirms the requirement of E-cadherin for SEPT7 distribution. Consistent with what was observed in X–Y confocal

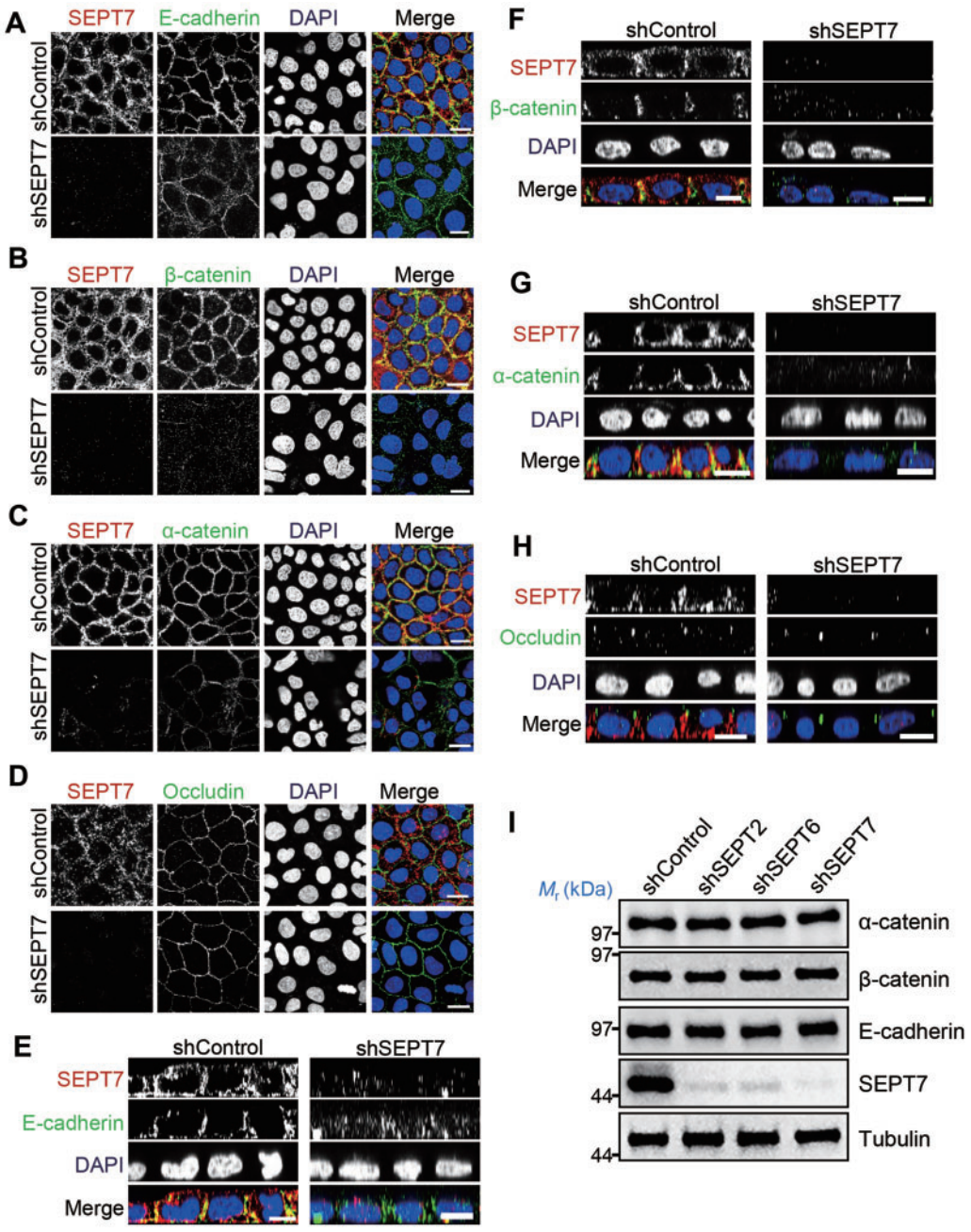

Figure 3 Septins are required for catenin maintenance but not tight junction. (**A**–**C**) Representative immunofluorescence staining of SEPT7 (red) and adherens junction proteins (green) E-cadherin (**A**), β-catenin (**B**), and α-catenin (**C**) in control and SEPT7-depleted monolayers. Caco-2 cells were infected with control shRNA or shSEPT7 lentivirus, respectively, and then plated onto coverslip to allow monolayer formation. Cells were fixed after 100% confluency followed by visualization using confocal microscopy. Note that cells become flatter and adherens junction proteins are diminished under depletion of SEPT7. A confocal section through the middle of monolayers is shown. Scale bar, 20 μm. (**D**) Representative maximum projections of Z-stack images of control and SEPT7-depleted Caco-2 monolayers. Cells labelled for SEPT7 (red) and the tight junction protein occludin (green) are shown. Scale bar, 20 μm. (**E**–**H**) The X–Z axis side views of monolayers from apical–basal membrane in **A**–**D** are shown. Confocal Z sections were taken along the entire depth of the monolayers and showed that SEPT7 apparently colocalizes with adherens junction proteins at lateral membrane. The staining of adherens junction proteins is diminished as the cells are depleted of SEPT7. However, tight junction protein localizes at apical–lateral membrane and keeps intact as SEPT7 is depleted. (**I**) Western blotting analyses of adherens junction proteins and tubulin in Caco-2 cells infected with control or shSEPT2/6/7 lentiviruses, respectively, in parallel with the immunofluorescence assays shown in **A**–**D**.

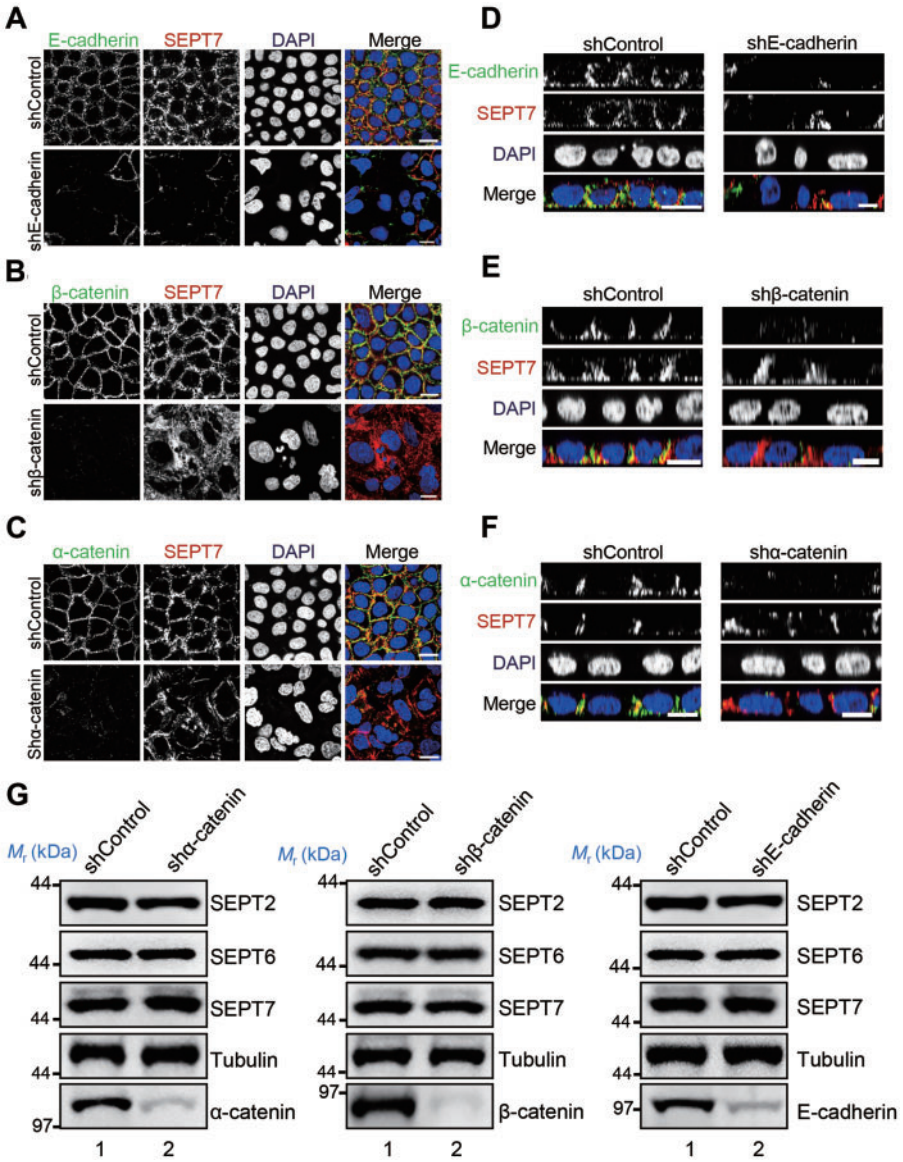

Figure 4 Junctional localization of septins depends on cadherin. (**A**) Representative immunofluorescence staining of SEPT7 (red) and E-cadherin (green) in control and E-cadherin-depleted monolayers. Caco-2 cells were infected with control shRNA or shE-cadherin lentivirus, respectively, and then plated onto coverslip to allow monolayer formation. Note that the staining of SEPT7 is diminished as E-cadherin is depleted. Scale bar, 20 μm. (**B**) Representative immunofluorescence staining of SEPT7 (red) and β-catenin (green) in control and β-catenin-depleted monolayers. Scale bar, 20 μm. (**C**) Representative immunofluorescence staining of SEPT7 (red) and α-catenin (green) in control and α-catenin-depleted monolayers. All of the above images were from a confocal section through the middle region of monolayers. Scale bar, 20 μm. (**D**–**F**) The X–Z axis side views of monolayers from apical–basal membrane shown in **A**–**C**. Confocal Z sections were taken along the entire depth of the monolayers and showed that the lateral localization of SEPT7 is dependent on E-cadherin rather than α/β-catenin. Scale bar, 20 μm. (**G**) Western blotting analyses of SEPT2, SEPT6, SEPT7, and tubulin in Caco-2 cells infected with control, shα-catenin, shβ-catenin, and shE-cadherin lentiviruses, respectively, in parallel with the immunofluorescence assays shown in **A**–**C**.

sections, suppression of β-catenin and α-catenin did not alter lateral localization of SEPT7 (Figure 4E and F). SEPT2 and SEPT6 have the same consequence as SEPT7 under suppression of E-cadherin, β-catenin, or α-catenin (Supplementary Figure S3). As a quality control, western blotting analyses confirmed that suppression of E-cadherin, β-catenin, or α-catenin did not alter the expression levels of SEPT2/6/7 proteins in the aforementioned experiments (Figure 4G). Thus, we conclude that the septin cytoskeleton localization to the lateral membrane is a function of E-cadherin.

Septin cytoskeleton recruits β-catenin to synergize with E-cadherin for functional adherens junction

The above immunofluorescence analyses indicate that the localization of SEPT2/6/7 depends on E-cadherin, while septin cytoskeleton is required for adherens junction assembly. We reason that SEPT7 may act as a scaffold for recruitment of α/β-catenin onto E-cadherin. To examine whether the interaction between E-cadherin and β-catenin is affected in the absence of septins, we carried out an immunoprecipitation assay of E-cadherin from Caco-2 cells treated with scramble shRNA and shSEPT2/6/7. As shown in Figure 5A, in the absence of SEPT7, the amount of β-catenin bound to E-cadherin was substantially reduced. Statistical analyses showed that removal of SEPT7 reduced the amount of β-catenin to 59% ± 4% coimmunoprecipitated with E-cadherin, and deletion of SEPT2 or SEPT6 likewise reduced the interaction between β-catenin and E-cadherin (Figure 5B), consistent with our hypothesis that septin cytoskeleton serves as a scaffold mediating the interaction between E-cadherin and α/β-catenin. To further examine whether septin cytoskeleton serves as a direct link between E-cadherin and β-catenin and evaluate the physical binding interface region of SEPT2/6/7 involved in this binding, we generated a series of SEPT truncation mutants for binding assays. As shown in Supplementary Figure S4A, GST-tagged E-cadherin cyto-domain and β-catenin proteins were used as matrices to absorb recombinant MBP-SEPT2/6/7 proteins purified from bacteria. As shown in Supplementary Figure S4B–D, SEPT2/6/7 proteins bind to β-catenin, while SEPT2 proteins exhibit strong binding to E-cadherin cyto-domain. Our analyses showed that the SEPT2/6/7 GTP-binding (M) domains physically interact with β-catenin. In addition, SEPT6/7 M domain showed weak binding to E-cadherin cyto-domain. Thus, we conclude that septin cytoskeleton physically interacts with E-cadherin and β-catenin and serves as a scaffold to stabilize the interaction of β-catenin and E-cadherin.

To assess the precise function of β-catenin–SEPT interaction in epithelial polarization, we engineered a competitive membrane-permeable peptide containing the M domain of SEPT2/6/7 (Figure 5C; Akram et al., 2018). As shown in Figure 5D, immunoprecipitation assay showed that TAT-GFP-SEPT2/6/7-M can compete with GFP-β-catenin and disrupt the β-catenin–SEPT association, while the negative control TAT-GFP did not interfere with the interaction between β-catenin and SEPT. To determine whether the β-catenin–SEPT interaction is required for adherens junction integrity and epithelial apical–basal polarity establishment, we treated cells with TAT-GFP-SEPT2/6/7-M and TAT-GFP, respectively, and allow cells to grow into monolayers. As expected, in the presence of 3 μM TAT-GFP-SEPT2/6/7-M, cells became flat and E-cadherin and β-catenin did not concentrate on cell junction compared with TAT-GFP group (Figure 5E and F). Thus, we conclude that the physical link between β-catenin and SEPT is important for epithelial lateral membrane integrity and apical–basal polarization.

Septins are necessary for efficient epithelial cell polarity/barrier formation

After demonstration of septin cytoskeleton in stabilizing adhesion junction complex in a biochemical assay, we next asked whether the interactions of SEPT2/6/7 with adherens junction are functionally important for epithelial polarity. To this end, transepithelial electrical resistance (TEER) assay was used to measure the para-cellular permeability in the absence of SEPT2/6/7 (illustrated in Figure 6A). In fully polarized Caco-2 monolayer, the TEER was 1400 $\Omega\,cm^2$. The resistance was abolished when Caco-2 cell monolayer was treated with FCF (Figure 6B). Similar perturbation of TEER was observed when actin cytoskeleton was perturbed by Latrunculin B (Lat.B), a chemical specifically perturbing actin filament. Interestingly, depolymerization of microtubule by Nocodazole did not compromise the TEER, suggesting that the adherens junction integrity is a function of actin and septin cytoskeleton but not microtubule network. Importantly, this chemical inhibition of septin filaments was reversible as removal of FCF resumed the transepithelial resistance, suggesting that septin filaments are essential for functional adherens junction. Our immunofluorescence analyses confirmed that both actin and SEPT2/6/7 are compromised in FCF-treated cells (Supplementary Figure S5A). Consistent with our hypothesis, removal of FCF restored the integrity of septin filaments (Supplementary Figure S5B).

To examine whether the compromised TEER is a specific function of perturbed association of septin filaments with E-cadherin, we carried out shRNA-mediated knockdown of SEPT2/6/7 and E-cadherin, respectively. The impacts of SEPT2/6/7 and E-cadherin deficiencies on Caco-2 polarity were assessed by TEER (Figure 6C). As shown in Figure 6D, control shRNA-treated Caco-2 cell monolayer exhibits typical measurement of TEER $\sim 1000\,\Omega\,cm^2$. However, Caco-2 cell monolayers depleted of SEPT2/6/7 exhibited much lower TEER with a mean value $\sim 600\,\Omega\,cm^2$. Polarized epithelial cells exhibit accurate plasticity as cells undergo polarization–depolarization cycle associated with cell division. To examine whether septin deficiency would alter the Caco-2 plasticity in polarization, Caco-2 cells grown in normal Dulbecco's modified Eagle medium (DMEM) were switched to low Ca^{2+} DMEM for 12 h. Those Caco-2 cells exhibited no connectivity or polarity as the TEER was zero. Moreover, cells were then switched to high Ca^{2+} DMEM to enable control shRNA-treated cells to establish contacts and connectivity. Consistent with the literature and experimental design, those control Caco-2 cells successfully established polarity and transepithelial resistance within 36 h of Ca^{2+} supplement as the TEER reached 1500 $\Omega\,cm^2$. However, the TEER of SEPT2/6/7-suppressed cells was capped at 600 $\Omega\,cm^2$ even with an extended period of time. The deficiency in TEER was also observed in E-cadherin-suppressed monolayers (Figure 6D). Thus, we conclude that SEPT2/6/7 filaments connect E-cadherin and synergize with catenin for functional adherens junction in polarized epithelial cells.

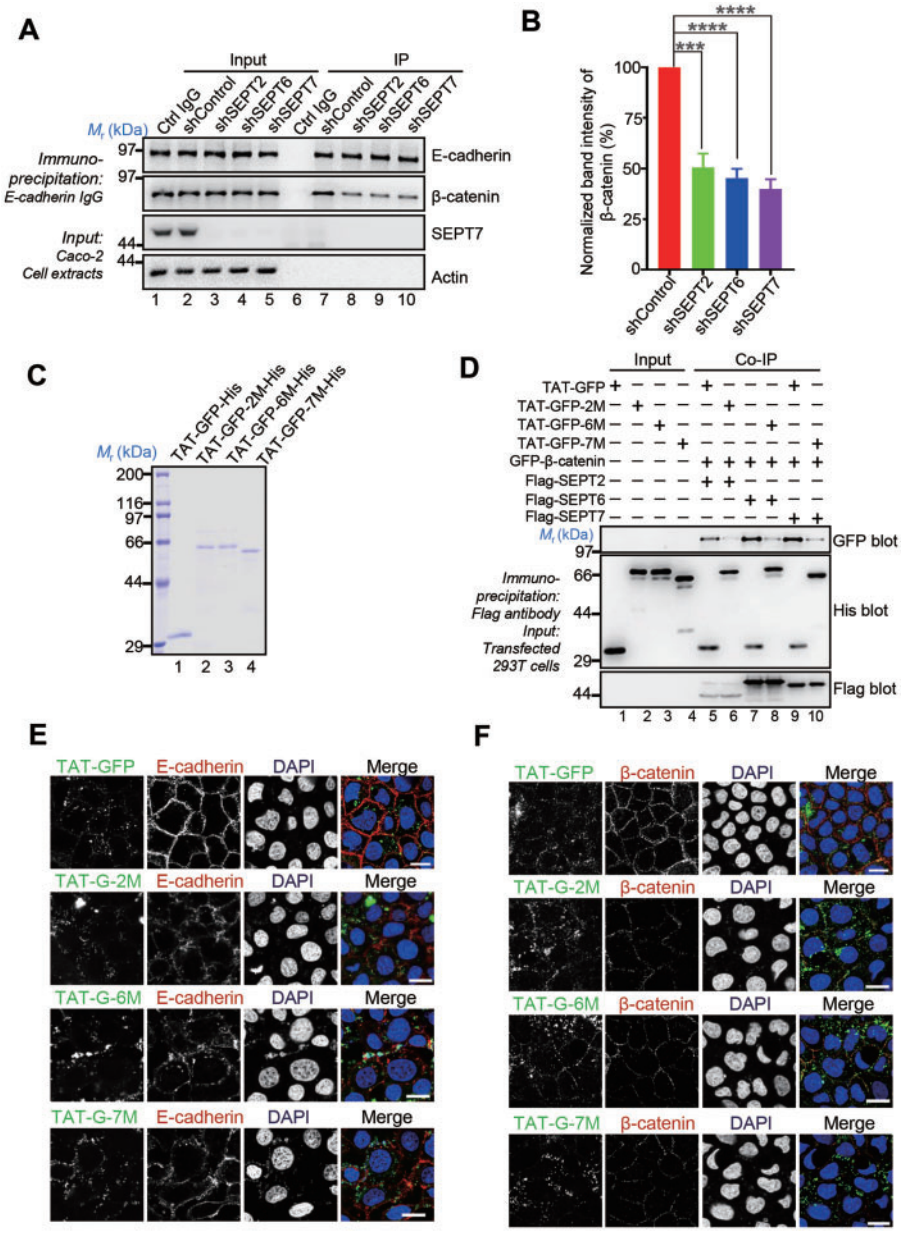

Figure 5 Septins recruit β-catenin to E-cadherin. (**A**) Caco-2 cells were transfected with control shRNA, shSEPT2, shSEPT6, and shSEPT7, respectively. Cells were harvested and subjected to immunoprecipitation with E-cadherin antibody or IgG, and the immunoprecipitates were separated by sodium dodecyl sulphate–polyacrylamide gel electrophoresis (SDS–PAGE) followed by western blotting using indicated antibodies. Note that E-cadherin brought down less β-catenin from SEPT2/6/7-depleted cells than control cells. (**B**) Quantitative analysis of the relative β-catenin intensity in shSEPT2/6/7 groups compared to control group. Data represent mean ± SEM from three independent experiments. Statistical significance was tested by two-sided *t*-test. ***$P < 0.001$, ****$P < 0.0001$. (**C**) Coomassie Brilliant Blue staining of SDS–PAGE gel was used to assess the quality and quantities of the purified recombinant peptides TAT-GFP-His, TAT-GFP-SEPT2-M-His (TAT-GFP-2M-His; amino acids 35–306), TAT-GFP-SEPT6-M-His (TAT-GFP-6M-His; amino acids 39–305), and TAT-GFP-SEPT7-M-His (TAT-GFP-7M-His; amino acids 31–296). (**D**) HEK293T cells expressing FLAG-SEPT2/6/7 and GFP-β-catenin were subjected to immunoprecipitation with FLAG antibody in the presence of TAT-GFP or TAT-GFP-SEPT2/6/7-M (TAT-GFP-2M/6M/7M) for overnight incubation and immunoblotted with His, FLAG, and GFP antibodies, respectively. Immunoblotting analysis showed that the interaction of β-catenin and SEPT2/6/7 was perturbed by the addition of TAT-GFP-SEPT2/6/7-M (TAT-GFP-2M/6M/7M). (**E** and **F**) Caco-2 monolayers were cultured to 70% confluence followed by introducing 3 μM TAT-GFP or TAT-GFP-SEPT2/6/7-M (TAT-G-2M/6M/7M) into DMEM at 37°C for overnight. Cells were fixed after 100% confluence followed by immunostaining with indicated antibodies. Note that the staining of β-catenin/E-cadherin is diminished upon SEPT2/6/7-M peptide competition.

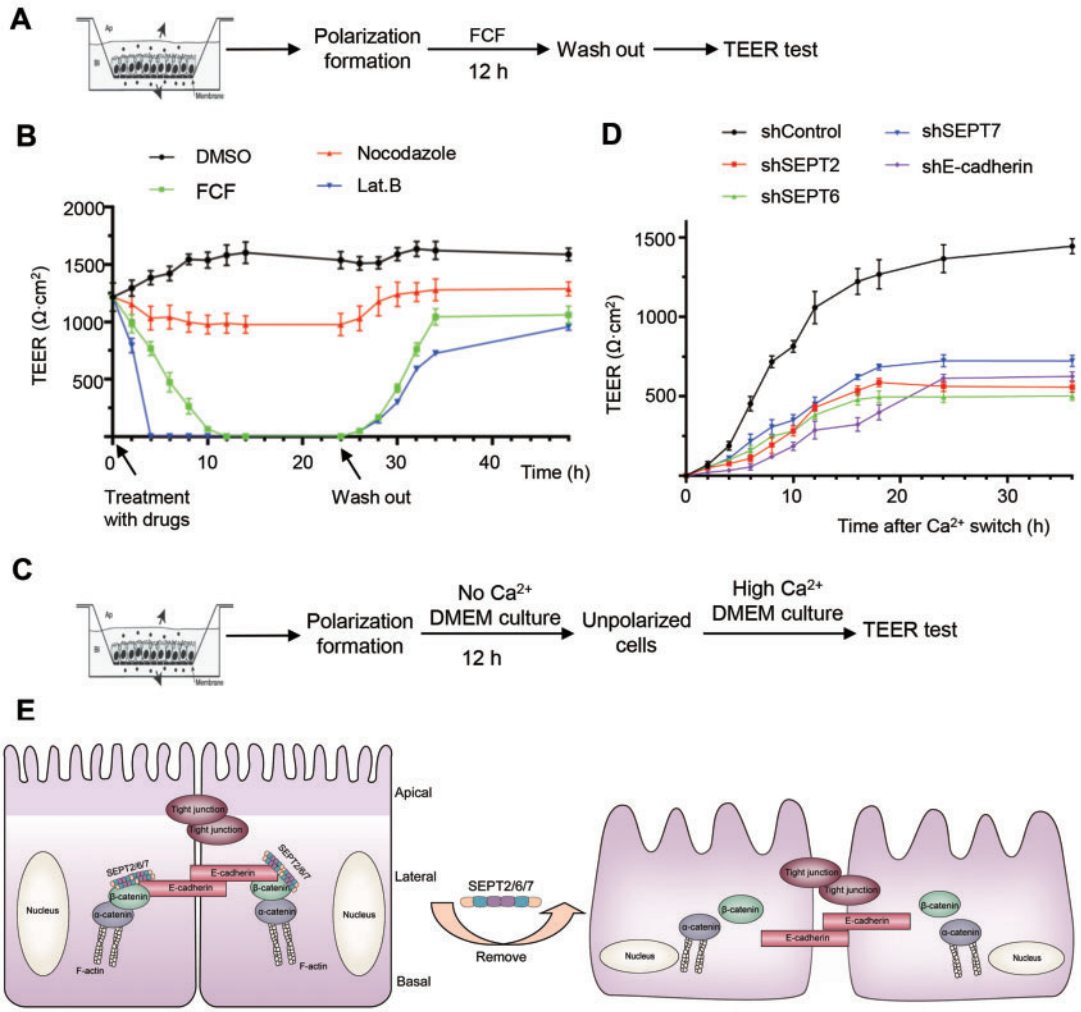

Figure 6 Septins are necessary for efficient epithelial cell polarity/barrier formation. (**A**) Schematic presentation of the method for TEER test of Caco-2 monolayers with drug treatment. Caco-2 single cells were plated onto transwell and grown for several days until confluent monolayers were established. After monolayers achieved maximal TEER, cells were treated with different drugs and TEER was monitored every 2 h. (**B**) Monolayers on transwell were treated with DMSO, FCF, Nocodazole, or Lat.B and TEER was monitored every 2 h. Data represent mean ± SEM from three independent experiments. (**C**) Schematic presentation of the method for TEER test of Caco-2 monolayers expressing control shRNA, shSEPT2, shSEPT6, or shSEPT7 under Ca^{2+} switch assay. Monolayers were cultured in Ca^{2+}-free minimum essential medium (MEM) with 10% dialyzed FBS for 16 h to break the Ca^{2+}-dependent cell junction and minimal TEER was achieved. Afterwards, the culture medium was changed to DMEM containing 10% fetal bovine serum (FBS) to reconstruct cell junction and TEER was monitored every 2 h. (**D**) Development of TEER after Ca^{2+} switch in control, SEPT2/6/7-depleted, and E-cadherin-depleted cells. Data represent mean ± SEM from three independent experiments. (**E**) Working model accounting for the function of septin cytoskeleton in epithelial apical–basal polarization and adherens junction integrity maintenance. SEPT2/6/7 filaments bind with E-cadherin and β-catenin directly to promote the stability of E-cadherin-dependent adherens junction at lateral membrane.

Discussion

We have shown that septin filaments physically interact with E-cadherin and are essential for a stable association of E-cadherin with α-catenin and β-catenin for stable hierarchical interactions in adherens complex formation and stability (Figure 6E). The failure of stable septin–adherens complex formation strongly indicates that septin filaments function in accurate adherens junction formation. This reinforces and extends previous observations of septin function in epithelial cell polarity establishment (Spiliotis et al., 2008; Founounou et al., 2013).

Actin cytoskeleton and microtubules are well known to provide the structural basis for epithelium polarity establishment (Li and Gundersen, 2008). Actin cytoskeleton develops regulatory molecule asymmetry distribution, while microtubules maintain the stability of the polarity protein organization (Hartsock and Nelson, 2008; Gavilan et al., 2015; Dogterom and Koenderink, 2019). Cell junctional complexes associated

with actin cytoskeleton and cell membrane provide contacts between neighboring epithelial cells and thus regulate epithelial barrier formation and control tissue architecture (Gibson and Perrimon, 2003; Harris and Tepass, 2010). Epithelial apicobasal axis orientation and organ culture are orchestrated by several polarity molecular pathways, e.g. par3–par6–aPKC polarity complex is activated by cdc42 and targeted to apical surface along with spindle bio-orientation completion (Jaffe et al., 2008; Qin et al., 2010; Xia et al., 2015) and subsequently stabilizes adherens junction and tight junction proteins to apical–lateral membrane (Aberle et al., 1994; Hartsock and Nelson, 2008; Nelson, 2009; Pinheiro and Bellaiche, 2018). Herein, we report that human SEPT2/6/7 filaments recruit E-cadherin to β-catenin to maintain adherens junction to cytoskeleton and establish apical–basal polarity. Loss of septin proteins results in epithelial barrier breakdown and polarity molecule distribution disorder.

In epithelial tissue morphogenesis, how cell apical–basal polarity is established and how single lumen is formed are fundamental questions. Using 2D and 3D cultured Caco-2 cells, we have demonstrated the functional relevance of septin filaments in epithelial cell polarization. Future studies will be required to delineate the mechanisms of action underlying septin–E-cadherin interaction using spectral imaging and superresolution imaging analyses (Xia et al., 2014; Liu et al., 2020a). We and colleagues had established the role of SEPT7–CENP-E in accurate chromosome segregation during mitosis (Spiliotis et al., 2005; Zhu et al., 2008). It would be of great interest to dissect the molecular machinery that links mitotic exit and cellular polarity establishment. The establishment of gastric organoids for studying mitotic chromosome movements and epithelial cell–pathogen interaction will enable us to study the hierarchical interactions of SEPT7/E-cadherin/β-catenin during mitotic exit and epithelial cell polarity establishment using gastric organoids (Yao and Smolka, 2019; Liu et al., 2020b).

In sum, we established an interrelationship between the SEPT2/6/7 complex and E-cadherin in the orchestration of epithelial cell polarity and connectivity. We propose that the SEPT2/6/7 complex forms a link between the assembly of adherens junctional complex and epithelial polarity via a direct SEPT7–E-cadherin contact. Because E-cadherin is absent from yeast, we reason that metazoans evolved an elaborate polarity establishment and maintenance machinery to ensure faithful cell–cell communication to orchestrate tissue homeostasis and faithful renewal in epithelial tissues.

Materials and methods

Cell culture and drug treatments

Caco-2 cells were purchased from the American Type Culture Collection and maintained as monolayers in advanced DMEM (Invitrogen) with 10% (*v*/*v*) FBS (HyClone) and 100 units/ml penicillin plus 100 μg/ml streptomycin (Invitrogen) at 37°C in a humidified atmosphere with 8% CO_2. The cells were routinely tested for mycoplasma contamination.

For 2D cell culture, Caco-2 cells were digested into single cells and 3×10^5 cells were plated onto coverslips in 24-well plates and overlaid with 500 μl medium. Cells were grown until 100% confluent.

For 3D cell culture, Caco-2 cells were digested into single cells and 5×10^4 cells were mixed with 30 μl ice-cold Matrigel (Corning) followed by plating on eight chambered coverglass (Thermo Fisher Scientific/Nunc). The mixture was incubated into 37°C to solidify for 15 min and overlaid with 250 μl medium. Cells were grown in gel for 6–8 days until cysts formed.

For drug treatment, septin assembly inhibitor FCF (Sigma 32974) was used at 100 μM for 12 h, Lat.B (Sigma) used at 10 μM for 12 h, and Nocodazole (Sigma) used at 10 μM for 12 h.

Plasmids and shRNA

To generate GST-tagged adherens junction proteins, polymerase chain reaction-amplified β-catenin and E-cadherin fragments were cloned into the pGEX-6P1 vector (GE Healthcare), while for different constructs expressing MBP-tagged septins with a C-terminal 6×His-tag, SEPT2, SEPT6, and SEPT7 truncation fragments were cloned into the pET30a-MBP vector (a gift from Prof. Tengchuan Jin at University of Science and Technology of China) by ClonExpress II One Step Cloning Kit (Vazyme). To generate TAT-GFP-SEPT2/6/7-M-His fusion proteins, an 11-amino acid TAT sequence followed by GFP and SEPT-M truncation was inserted into the pET-22b vector. TAT-GFP-His and TAT-GFP-SEPT-M-His fusion proteins were expressed and purified as described previously.

For endogenous gene knockdown experiments, shRNA sequences were inserted into the lentivirus-based PLKO.1 vector via *Eco*RI and *Age*I sites. The following sequences target different genes: *shSEPT2*: 5′-GGTGAATATTGTGCCTGTCAT-3′; *shSEPT6*: 5′-CCTGAAGTCTCTGGACCTAGT-3′; *shSEPT7*: 5′-CTTGCAGCTGTGACTTATAAT-3′; *shβ-catenin*: 5′-GCTTGGAATGAGACTGCTGAT-3′; *shα-catenin*: 5′-GGACCTGCTTTCGGAGTACAT-3′; *shE-cadherin:* 5′-GCACGTACACAGCCCTAAT-3′.

Antibodies

Rabbit anti-SEPT2 (ab88657; 1:1000 for western blotting (WB); 1:200 for immunofluoresence (IF)), anti-SEPT6 (ab138036; 1:1000 for WB; 1:200 for IF), and anti-SEPT7 (ab18602; 1:1000 for WB; 1:200 for IF) antibodies were from Abcam. Mouse anti-β-catenin (sc-7963; 1:1000 for WB; 1:200 for IF) antibody was from Santa Cruz. Rabbit anti-β-catenin (8480; 1:400 for IF), mouse anti-E-cadherin (14472; 1:1000 for WB; 1:400 for IF), Alexa Fluor 555-Phalloidin (8953; 1:5000 for IF), and anti-MBP-tag (2396; 1:2000 for WB) antibodies were from Cell Signaling Technology. Mouse anti-occludin (33-1500; 1:400 for IF) and anti-α-catenin (13-9700; 1:1000 for WB; 1:400 for IF) antibodies were from Thermo Fisher Scientific. Mouse anti-α-tubulin (T9017; 1:2000 for WB) and anti-α-tubulin-FITC (F2168; 1:5000 for IF) antibodies were from Sigma. Mouse anti-ezrin (610602; 1:2000 for WB; 1:400 for IF) was

form BD Biosciences. Secondary antibodies were from Jackson Immune Research Laboratory.

TEER

For TEER measurement, 3×10^5 cells were plated onto a 1.12-cm^2 surface area of 0.4-μm-pore translucent polyester membrane transwell inserts (Corning, 3460). After 3–4 days, confluent monolayers were established and TEER was measured by Millicell ERS-2 instrument (Millipore). For drug treatment experiment, after monolayers achieved maximal TEER, cells were treated with different drugs and TEER was monitored every 2 h. For Ca^{2+} switch experiment, confluent monolayers were cultured in Ca^{2+}-free MEM with 10% dialyzed FBS for 16 h to break the Ca^{2+}-dependent cell junction and achieve minimal TEER before changing medium with DMEM containing 10% FBS to reconstruct cell junction and monitor TEER every 2 h. The unit of TEER value is Ω cm, which was obtained by subtracting membrane blank value and multiplying the surface area of the insert.

Lentiviral infection

The lentivirus-based vector PLKO.1, psPAX2, and pMD2.G were ordered from Addgene. Lentivirus packaging was performed by using Max PEI-based cotransfection of HEK293T cells with psPAX2, pMD2.G, and the lentiviral vector PLKO.1. Supernatant medium of packaging cells was harvested up to 48 h of transfection and filtered through a 0.22-μm filter. For infection, Caco-2 cells were cultured in DMEM with virus at the ratio of 1:1 and supplemented with 8 μg/ml polybrene (Sigma) and incubated for 12 h. Afterwards, the culture medium was changed to DMEM containing 10% FBS followed by selection with puromycin.

Immunoprecipitation and western blotting

For immunoprecipitation, Caco-2 cells depleted of endogenous septins were harvested and lysed in RIPA buffer (20 mM Tris–HCl, pH 7.5, 150 mM NaCl, 1% Triton X-100, 0.5% sodium deoxycholate, 0.1% SDS, and 2 mM EDTA) supplemented with protease inhibitor cocktail (Sigma). After pre-clearing with protein A/G resin, the lysate was incubated with E-cadherin antibody at 4°C for 24 h with gentle rotation. Protein A/G resin was then added to the lysates, and they were incubated for another 6 h. The Protein A/G resin was then spun down and washed three times with RIPA buffer before being resolved by SDS–PAGE, and then proteins were transferred onto nitrocellulose membrane and immunoblotted with the indicated antibodies. For FLAG-tagged protein immunoprecipitation, the FLAG-M2 resin was added to the lysates and incubated for 4 h before washing. The intensity of bands was quantified by Image J.

Recombinant protein preparation and GST pull-down assay

The plasmids of GST-fusion, His-MBP-tagged proteins were transformed into *Escherichia coli* strain BL21 or Rosetta (DE3), and protein expression was induced with 0.2 mM isopropylthio-β-galactoside, with shaking overnight at 16°C for 20 h. Bacteria expressing MBP-SEPT-His_6 fusion proteins were suspended and lysed by sonication in Ni-NTA binding buffer (50 mM NaH_2PO_4, pH 8.0, 300 mM NaCl, and 10 mM imidazole) with protease inhibitor cocktail and 1 μg/ml PMSF and incubated with Ni-NTA agarose (Qiagen) for 1 h at 4°C. The agarose was washed three times in Ni-NTA binding buffer and eluted with Ni-NTA binding buffer supplemented with 250 mM imidazole.

Bacteria expressing GST-fusion proteins were suspended and lysed by sonication in phosphate-buffered saline (PBS) supplemented with protease inhibitor cocktail and 1% Triton X-100. The preparation was incubated with Glutathione-Sepharose 4B (GE Healthcare Life Science) for 1 h at 4 °C. The resin was washed three times.

For GST pull-down assay, GST and GST-tagged fusion proteins-bound glutathione beads were incubated with purified and eluted MBP-SEPT-His_6 fusion in pull-down buffer (50 mM Tris–Cl, pH 8.0, 50 mM NaCl, 0.5 mM EDTA, 1 mM DTT, and 5% glycerol) with protease inhibitor cocktail plus 0.1% Triton X-100 for 4 h at 4°C. The resins were washed three times with pull-down buffer containing 0.2% Triton X-100, followed by boiling in SDS-sample buffer. The samples were subjected to SDS–PAGE gel and western blotting detection using an anti-MBP antibody.

Purification of recombinant TAT-GFP proteins and interrogation of SEPT–β-catenin in vivo

For directly assessing the functional importance of the SEPT–β-catenin interaction in adherens junction integrity, a membrane-permeable peptide containing SEPT amino acids involving binding interface between SEPT and β-catenin was constructed as previously described (Cao et al., 2015; Adams et al., 2016; Akram et al., 2018). Caco-2 cells were cultured to 70% confluency before introducing TAT-GFP-SEPT2/6/7-M peptide into medium, with an optimal concentration at 3 μM. The treated cells were fixed after reaching 100% confluency and permeabilized followed by immunofluorescence staining.

Purification of recombinant proteins was carried out as described previously (Akram et al., 2018). Briefly, the His fusion proteins from bacteria in the soluble fraction were purified using Ni-NTA agarose (Qiagen). To test the efficacy of SEPT-M peptide, 293T cells expressing FLAG-SEPT2/6/7 and GFP-β-catenin were subjected to immunoprecipitation with FLAG antibody in the presence of TAT-GFP or TAT-GFP-SEPT2/6/7-M peptide for overnight and immunoblotted with His, FLAG, and GFP antibodies, respectively.

Immunofluorescence

For visualization and quantitative analyses, monolayers and 3D Caco-2 cysts were fixed with PBS containing 3.7% paraformaldehyde for 10 min followed by permeabilization with 0.2% Triton X-100 for 3 min. After blocking with the PBS with 0.05%

Tween-20 buffer containing 1% bovine serum albumin (Sigma) for 1 h at room temperature, the fixed cells were incubated with primary antibodies in a humidified chamber for 1 h at room temperature or overnight at 4°C, followed by secondary antibodies for 1 h at 37°C. The DNA was stained with 4′,6-diamidino-2-phenylindole (DAPI) (Sigma). All images were collected using a Zeiss laser-scanning confocal microscope (Zeiss LSM 880). To generate side views of 2D monolayers, fixed and stained samples were scanned every 0.5 μm at Z axis from apical to basal membrane and reconstructed by LSM 880 microscope. The laser wavelengths used were 405, 488, and 561 nm and the laser intensity was kept to a minimum. Images analysis and fluorescence intensity measurements were performed with ZEN software and Image J.

Statistics

All statistics are described in the figure legends. Two-sided unpaired Student's *t*-test was applied for experimental comparisons, using GraphPad Prism. All western blotting analyses were taken from three separated experiments. No statistical method was used to predetermine sample size. All data were expected to have normal distribution.

Supplementary material

Supplementary material is available at *Journal of Molecular Cell Biology* online.

Acknowledgements

We thank our laboratory members for inspiring discussion during the course of this study.

Funding

This work was supported in part by grants from the National Natural Science Foundation of China (31621002, 32090040, 21922706, 91854203, 91853115, 81630080, 31430054, and 31671405), National Key Research and Development Program of China (2017YFA0503600, 2016YFA0100500, and 2016YFA0101200), the Ministry of Education (IRT_17R102, 20113402130010), the Strategic Priority Research Program of Chinese Academy of Sciences (XDB19000000), the Fundamental Research Funds for the Central Universities (WK2340000066 and WK2070000194), and National Institutes of Health Grants (CA164133, DK115812, and DK56292).

Conflict of interest: none declared.

References

Aberle, H., Butz, S., Stappert, J., et al. (1994). Assembly of the cadherin–catenin complex in vitro with recombinant proteins. J. Cell Sci. *107*, 3655.

Adams, G., Jr, Zhou, J., Wang, W., et al. (2016). The microtubule plus end tracking protein TIP150 interacts with cortactin to steer directional cell migration. J. Biol. Chem. *291*, 20692–20706.

Akram, S., Yang, F., Li, J., et al. (2018). LRIF1 interacts with HP1α to coordinate accurate chromosome segregation during mitosis. J. Mol. Cell Biol. *10*, 527–538.

Bisaria, A., Hayer, A., Garbett, D., et al. (2020). Membrane-proximal F-actin restricts local membrane protrusions and directs cell migration. Science *368*, 1205–1210.

Boubakar, L., Falk, J., Ducuing, H., et al. (2017). Molecular memory of morphologies by septins during neuron generation allows early polarity inheritance. Neuron *95*, 834–851.e5.

Bowen, J.R., Hwang, D., Bai, X., et al. (2011). Septin GTPases spatially guide microtubule organization and plus end dynamics in polarizing epithelia. J. Cell Biol. *194*, 187–197.

Bryant, D.M., and Mostov, K.E. (2008). From cells to organs: building polarized tissue. Nat. Rev. Mol. Cell Biol. *9*, 887–901.

Campos, Y., Qiu, X., Gomero, E., et al. (2016). Alix-mediated assembly of the actomyosin–tight junction polarity complex preserves epithelial polarity and epithelial barrier. Nat. Commun. *7*, 11876.

Cao, D., Su, Z., Wang, W., et al. (2015). Signaling scaffold protein IQGAP1 interacts with microtubule plus-end tracking protein SKAP and links dynamic microtubule plus-end to steer cell migration. J. Biol. Chem. *290*, 23766–23780.

Dogterom, M., and Koenderink, G.H. (2019). Actin–microtubule crosstalk in cell biology. Nat. Rev. Mol. Cell Biol. *20*, 38–54.

Founounou, N., Loyer, N., and Le Borgne, R. (2013). Septins regulate the contractility of the actomyosin ring to enable adherens junction remodeling during cytokinesis of epithelial cells. Dev. Cell *24*, 242–255.

Gavilan, M.P., Arjona, M., Zurbano, A., et al. (2015). Alpha-catenin-dependent recruitment of the centrosomal protein CAP350 to adherens junctions allows epithelial cells to acquire a columnar shape. PLoS Biol. *13*, e1002087.

Gibson, M.C., and Perrimon, N. (2003). Apicobasal polarization: epithelial form and function. Curr. Opin. Cell Biol. *15*, 747–752.

Harris, T.J., and Tepass, U. (2010). Adherens junctions: from molecules to morphogenesis. Nat. Rev. Mol. Cell Biol. *11*, 502–514.

Hartsock, A., and Nelson, W.J. (2008). Adherens and tight junctions: structure, function and connections to the actin cytoskeleton. Biochim. Biophys. Acta *1778*, 660–669.

Hu, Q., Nelson, W.J., and Spiliotis, E.T. (2008). Forchlorfenuron alters mammalian septin assembly, organization, and dynamics. J. Biol. Chem. *283*, 29563–29571.

Jaffe, A.B., Kaji, N., Durgan, J., et al. (2008). Cdc42 controls spindle orientation to position the apical surface during epithelial morphogenesis. J. Cell Biol. *183*, 625–633.

Kim, J., and Cooper, J.A. (2018). Septins regulate junctional integrity of endothelial monolayers. Mol. Biol. Cell *29*, 1693–1703.

Kinoshita, M. (2003). The septins. Genome Biol. *4*, 236.

Kremer, B.E., Adang, L.A., and Macara, I.G. (2007). Septins regulate actin organization and cell-cycle arrest through nuclear accumulation of NCK mediated by SOCS7. Cell *130*, 837–850.

Kremer, B.E., Haystead, T., and Macara, I.G. (2005). Mammalian septins regulate microtubule stability through interaction with the microtubule-binding protein MAP4. Mol. Biol. Cell *16*, 4648–4659.

Li, R., and Gundersen, G.G. (2008). Beyond polymer polarity: how the cytoskeleton builds a polarized cell. Nat. Rev. Mol. Cell Biol. *9*, 860–873.

Liu, D., Ge, L., Wang, F., et al. (2007). Single-molecule detection of phosphorylation-induced plasticity changes during ezrin activation. FEBS Lett. *581*, 3563–3571.

Liu, X., Liu, X., Wang, H., et al. (2020a). Phase separation drives decision making in cell division. J. Biol. Chem. *295*, 13419–13431.

Liu, X., Xu, L., Li, J., et al. (2020b). Mitotic motor CENP-E cooperates with PRC1 in temporal control of central spindle assembly. J. Mol. Cell Biol. *12*, 654–665.

McCaffrey, L.M., and Macara, I.G. (2011). Epithelial organization, cell polarity and tumorigenesis. Trends Cell Biol. *21*, 727–735.

McMurray, M.A., and Thorner, J. (2009). Septins: molecular partitioning and the generation of cellular asymmetry. Cell Div. *4*, 18.

Mostowy, S., and Cossart, P. (2012). Septins: the fourth component of the cytoskeleton. Nat. Rev. Mol. Cell Biol. *13*, 183–194.

Nelson, W.J. (2009). Remodeling epithelial cell organization: transitions between front–rear and apical–basal polarity. Cold Spring Harb. Perspect. Biol. *1*, a000513.

Neubauer, K., and Zieger, B. (2017). The mammalian septin interactome. Front. Cell Dev. Biol. *5*, 3.

O'Brien, L.E., Zegers, M.M., and Mostov, K.E. (2002). Opinion: building epithelial architecture: insights from three-dimensional culture models. Nat. Rev. Mol. Cell Biol. *3*, 531–537.

Odenwald, M.A., Choi, W., Buckley, A., et al. (2017). ZO-1 interactions with F-actin and occludin direct epithelial polarization and single lumen specification in 3D culture. J. Cell Sci. *130*, 243–259.

Pinheiro, D., and Bellaiche, Y. (2018). Mechanical force-driven adherens junction remodeling and epithelial dynamics. Dev. Cell *47*, 3–19.

Pous, C., Klipfel, L., and Baillet, A. (2016). Cancer-related functions and subcellular localizations of septins. Front. Cell Dev. Biol. *4*, 126.

Qin, Y., Meisen, W.H., Hao, Y., et al. (2010). Tuba, a Cdc42 GEF, is required for polarized spindle orientation during epithelial cyst formation. J. Cell Biol. *189*, 661–669.

Rodriguez-Boulan, E., and Macara, I.G. (2014). Organization and execution of the epithelial polarity programme. Nat. Rev. Mol. Cell Biol. *15*, 225–242.

Sellin, M.E., Holmfeldt, P., Stenmark, S., et al. (2011). Microtubules support a disk-like septin arrangement at the plasma membrane of mammalian cells. Mol. Biol. Cell *22*, 4588–4601.

Sidhaye, V.K., Chau, E., Breysse, P.N., et al. (2011). Septin-2 mediates airway epithelial barrier function in physiologic and pathologic conditions. Am. J. Respir. Cell Mol. Biol. *45*, 120–126.

Sirajuddin, M., Farkasovsky, M., Hauer, F., et al. (2007). Structural insight into filament formation by mammalian septins. Nature *449*, 311–315.

Sousa, B., Pereira, J., and Paredes, J. (2019). The crosstalk between cell adhesion and cancer metabolism. Int. J. Mol. Sci. *20*, 1933.

Spiliotis, E.T., Hunt, S.J., Hu, Q., et al. (2008). Epithelial polarity requires septin coupling of vesicle transport to polyglutamylated microtubules. J. Cell Biol. *180*, 295–303.

Spiliotis, E.T., Kinoshita, M., and Nelson, W.J. (2005). A mitotic septin scaffold required for mammalian chromosome congression and segregation. Science *307*, 1781–1785.

Torraca, V., and Mostowy, S. (2016). Septins and bacterial infection. Front. Cell Dev. Biol. *4*, 127.

Xia, J., Swiercz, J.M., Banon-Rodriguez, I., et al. (2015). Semaphorin–plexin signaling controls mitotic spindle orientation during epithelial morphogenesis and repair. Dev. Cell *33*, 299–313.

Xia, P., Liu, X., Wu, B., et al. (2014). Superresolution imaging reveals structural features of EB1 in microtubule plus-end tracking. Mol. Biol. Cell *25*, 4166–4173.

Yao, X., Cheng, L., and Forte, J.G. (1996). Biochemical characterization of ezrin–actin interaction. J. Biol. Chem. *271*, 7224–7229.

Yao, X., and Smolka, A.J. (2019). Gastric parietal cell physiology and Helicobacter pylori-induced disease. Gastroenterology *156*, 2158–2173.

Zheng, S., Dong, F., Rasul, F., et al. (2018). Septins regulate the equatorial dynamics of the separation initiation network kinase Sid2p and glucan synthases to ensure proper cytokinesis. FEBS J. *285*, 2468–2480.

Zhu, M., Wang, F., Yan, F., et al. (2008). Septin 7 interacts with centromere-associated protein E and is required for its kinetochore localization. J. Biol. Chem. *283*, 18916–18925.